

The British University in Egypt

**BUE Scholar**

---

Pharmacy

Health Sciences

---

1-2023

## Elafibranor modulates ileal macrophage polarization to restore intestinal integrity in NASH: Potential crosstalk between ileal IL-10/STAT3 and hepatic TLR4/NF- $\kappa$ B axes

Andrew Hakeem

*The British University in Egypt*

Mohamed M. Kamal

*The British University in Egypt, mohamed.kamal@bue.edu.eg*

Rasha A. Radwan

*Sinai University*


Basma A. AbdelRahman

*The British University in Egypt, basma.alaa@bue.edu.eg*

Olfat A. Hammam

*Theodor Bilharz Research Institute*

Follow this and additional works at: <https://buescholar.bue.edu.eg/pharmacy>

 *next page for additional authors*

Part of the [Digestive System Diseases Commons](#), [Immunity Commons](#), and the [Other Pharmacy and Pharmaceutical Sciences Commons](#)

---

### Recommended Citation

Hakeem, Andrew; Kamal, Mohamed M.; Radwan, Rasha A.; AbdelRahman, Basma A.; Hammam, Olfat A.; Elmazar, Mohey M.; El-Khatib, Aiman S.; and Attia, Yasmeen M., "Elafibranor modulates ileal macrophage polarization to restore intestinal integrity in NASH: Potential crosstalk between ileal IL-10/STAT3 and hepatic TLR4/NF- $\kappa$ B axes" (2023). *Pharmacy*. 662.

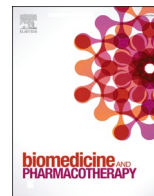
<https://buescholar.bue.edu.eg/pharmacy/662>

This Article is brought to you for free and open access by the Health Sciences at BUE Scholar. It has been accepted for inclusion in Pharmacy by an authorized administrator of BUE Scholar. For more information, please contact [bue.scholar@gmail.com](mailto:bue.scholar@gmail.com).

---

## **Authors**

Andrew Hakeem, Mohamed M. Kamal, Rasha A. Radwan, Basma A. AbdelRahman, Olfat A. Hammam, Mohey M. Elmazar, Aiman S. El-Khatib, and Yasmeen M. Attia



# Elafibranor modulates ileal macrophage polarization to restore intestinal integrity in NASH: Potential crosstalk between ileal IL-10/STAT3 and hepatic TLR4/NF- $\kappa$ B axes

Andrew N. Hakeem<sup>a,b</sup>, Mohamed M. Kamal<sup>b,c,d</sup>, Rasha A. Tawfiq<sup>a,b</sup>, Basma A. Abdelrahman<sup>a,b</sup>, Olfat A. Hammam<sup>e</sup>, Mohamed M. Elmazar<sup>a,b</sup>, Aiman S. El-Khatib<sup>f</sup>, Yasmeen M. Attia<sup>a,b,\*</sup>

<sup>a</sup> Department of Pharmacology, Faculty of Pharmacy, The British University in Egypt, Cairo, Egypt

<sup>b</sup> The Center for Drug Research and Development (CDRD), Faculty of Pharmacy, The British University in Egypt, Cairo, Egypt

<sup>c</sup> Department of Biochemistry, Faculty of Pharmacy, Ain Shams University, Cairo, Egypt

<sup>d</sup> Department of Biochemistry, Faculty of Pharmacy, The British University in Egypt, Cairo, Egypt

<sup>e</sup> Department of Pathology, Theodor Bilharz Research Institute, Giza, Egypt

<sup>f</sup> Department of Pharmacology and Toxicology, Faculty of Pharmacy, Cairo University, Cairo, Egypt

## ARTICLE INFO

### Keywords:

NASH  
Intestinal permeability  
PPAR  
Macrophage polarization  
TLR4  
STAT3

## ABSTRACT

Experimental and clinical evidence implicate disrupted gut barrier integrity in provoking innate immune responses, specifically macrophages, towards the progression of non-alcoholic steatohepatitis (NASH). Peroxisome proliferator-activated receptors (PPARs), a subset of the nuclear receptor superfamily, act to fine-tune several metabolic and inflammatory processes implicated in NASH. As such, the current study was carried out to decipher the potential role of dual PPAR  $\alpha/\delta$  activation using elafibranor (ELA) on ileal macrophage polarization (MP) and its likely impact on the liver in a NASH setting. To achieve this aim, an *in vitro* NASH model using fat-laden HepG2 cells was first used to validate the impact of ELA on hepatic fat accumulation. Afterwards, ELA was used in a combined model of dietary NASH and chronic colitis analogous to the clinical presentation of NASH parallel with intestinal barrier dysfunction. ELA mitigated fat accumulation *in vitro* as evidenced by Oil Red-O staining and curbed triglyceride levels. Additionally, ELA restored the expression of tight junctional proteins, claudin-1 and occludin, along with decreasing intestinal permeability and inflammation skewing ileal macrophages towards the M2 phenotype, as indicated by boosted arginase-1 (Arg1) and curtailed inducible nitric oxide synthase (iNOS) expression levels. These changes were aligned with a modulation in hepatic toll-like receptor-4 (TLR4)/nuclear factor kappa B (NF- $\kappa$ B) along with ileal interleukin-10 (IL-10)/signal transducer and activator of transcription-3 (STAT3) axes. Overall, the present findings suggest that the dual PPAR  $\alpha/\delta$  agonist, ELA, may drive MP in the ileum towards the M2 phenotype improving intestinal integrity towards alleviating NASH.

## 1. Introduction

The widespread global prevalence of non-alcoholic fatty liver disease (NAFLD) and the critical clinical outcomes associated with its more progressive form, non-alcoholic steatohepatitis (NASH), pose a global

economic burden and entail an alarming health need that is yet to be met [1]. Once believed to be merely a product of two subsequent metabolic and inflammatory hits, it is now appreciated that diverse local and extrahepatic pathogenic processes converge into NASH progression [2]. A subset of NASH patients exhibits pathological alterations in the

**Abbreviations:** Arg1, Arginase-1; BSA, Bovine serum albumin; DMEM, Dulbecco's Modified Eagle Medium; DMSO, dimethyl sulfoxide; DSS, Dextran sodium sulfate; ELA, Elafibranor; FFA, Free fatty acids; FITC, Fluorescein isothiocyanate; HFD, High fat diet; IFN $\gamma$ , Interferon-gamma; IL-10, Interleukin-10; iNOS, Inducible nitric oxide synthase; I $\kappa$ B $\alpha$ , Inhibitor of kappa B-alpha; IKK, inhibitor of kappa-B kinase; LBP, Lipopolysaccharide-binding protein; LPS, Lipopolysaccharide; MP, Macrophage polarization; NAFLD, Non-alcoholic fatty liver disease; NASH, Non-alcoholic steatohepatitis; NF- $\kappa$ B, Nuclear factor kappa B; OA, Oleic acid; PA, Palmitic acid; PPAR, Peroxisome proliferator-activated receptor; STAT3, Signal transducer and activator of transcription-3; TG, Triglycerides; TLR4, Toll-like receptor-4.

\* Correspondence to: Department of Pharmacology, The Center for Drug Research and Development (CDRD), Faculty of Pharmacy, The British University in Egypt, Suez Desert Road, P.O. Box 43, El-Sherouk City, Cairo 11837, Egypt.

E-mail address: [yasmeen.attia@bue.edu.eg](mailto:yasmeen.attia@bue.edu.eg) (Y.M. Attia).

<https://doi.org/10.1016/j.bioph.2022.114050>

Received 5 August 2022; Received in revised form 17 November 2022; Accepted 25 November 2022

Available online 30 November 2022

0753-3322/© 2022 The Authors. Published by Elsevier Masson SAS. This is an open access article under the CC BY-NC-ND license (<http://creativecommons.org/licenses/by-nc-nd/4.0/>).

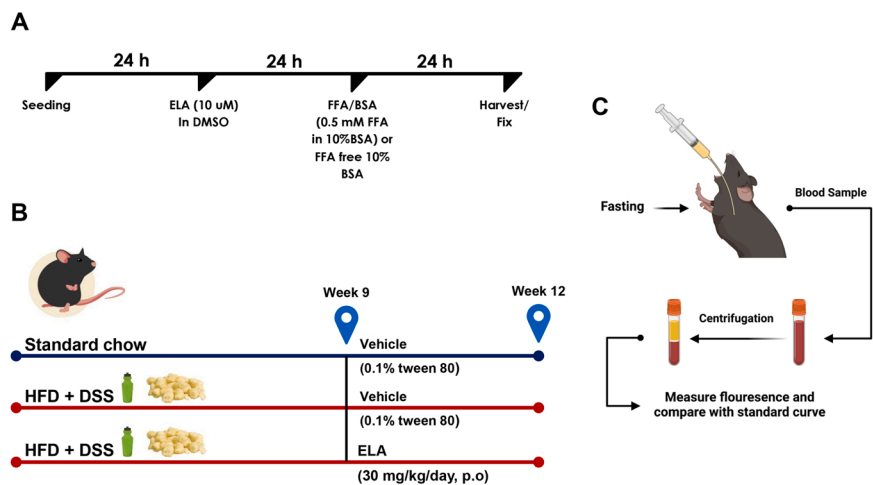


**Fig. 1.** Experimental design and timeline of *in vitro* and *in vivo* studies and FITC-dextran intestinal permeability assay. (A) For *in vitro* investigations, HepG2 cells were seeded on the first day in complete media, treated with elafibranor (ELA, 10  $\mu$ M) or an equivalent volume of DMSO on the second day. On the third day, cells were challenged with 0.5 mM free fatty acid (FFA) mixture of oleic/palmitic acids at a ratio of 2:1, or an equivalent volume of FFA-free bovine serum albumin (BSA). On the fourth and final day, cells were either fixed with 10% formalin and subsequently stained with lipophilic Oil Red-O or harvested for determination of triglyceride (TG) and protein content. (B) For *in vivo* investigations, C57BL/6 male mice were randomly allocated into 3 experimental groups. The first group was maintained on standard chow diet, the second and third groups received a high fat diet (HFD) and 0.5% dextran sodium sulfate (DSS) supplemented in drinking water. ELA was administered at a dose of 30 mg/kg, p.o. after 8 weeks of induction for a duration of 4 weeks. (C) For the intestinal permeability assay, mice were orally administered fluorescein isothiocyanate (FITC)-dextran after being challenged with a four-hour food deprivation period with free

access to water. Four hours later, FITC-dextran concentrations were estimated in serum samples to assess intestinal permeability.

gut-liver axis manifested in dysbiosis, compromised barrier integrity, and bacterial translocation [3]. Experimental and clinical evidence suggest that bacterial products translocated from a failing gut barrier is one of the key mechanisms contributing to the systemic low-grade inflammation present in NASH [4].

Mirroring the T helper-1 and -2 polarization states, macrophages are known to alternate between two phenotypes, *viz.*, the classical M1 and alternative M2. These phenotypes depict both extremes of the macrophage polarization (MP) programs where the pro-inflammatory M1 macrophages lie on one end whereas the tempered, tissue repairing, and anti-inflammatory M2 lie on the other [5]. One of the well-characterized paradigms explaining the gut-liver crosstalk is that of the toll-like receptor-4 (TLR4) where lipopolysaccharides (LPS) crossing the gut barrier and translocating to the hepatic tissue become recognized by TLR4 expressed by the liver parenchyma and innate immune cells [6]. Engaging hepatic TLR4 by the translocated LPS leads to downstream activation of nuclear factor kappa B (NF- $\kappa$ B), a master regulator of the M1 program in macrophages that controls the secretion of several pro-inflammatory cytokines implicated in NASH [5,6]. The notion that therapeutic modalities targeting TLR4/NF- $\kappa$ B signaling might be beneficial in NASH is supported by experimental evidence showing that mice with genetic defects in TLR4 [7] and NF- $\kappa$ B [8] are protected from diet-induced liver injury. This is further supported by clinical data showing higher expression of TLR4 [9] and NF- $\kappa$ B [10] in NASH liver biopsies. Clinical data also suggest that alterations in barrier integrity may be linked to TLR4/NF- $\kappa$ B hepatic signaling and the severity of NASH progression [6].

Barrier integrity and intestinal homeostasis are maintained through complex interactions between different epithelial and immune cells that also include macrophages as profound influencers [11]. Overwhelming evidence supports the notion that polarizing lamina propria macrophages towards an anti-inflammatory M2 phenotype confers protection against intestinal insults [12,13]. While this concept has been well validated in experimental models of colitis, it was not extensively explored in a NASH setting. Nevertheless, these macrophages are known to be extremely malleable by the repertoire of signals present in their milieu. On one hand, T helper-1-derived interferon-gamma (IFN $\gamma$ ) and LPS-triggered TLR4 synergize for robust engagement of the aggressive M1 phenotype [14] that is known to wreak havoc on the intestinal barrier through inducible nitric oxide synthase (iNOS)-mediated production of highly noxious nitric oxide (NO) and the secretion of several pro-inflammatory cytokines [15]. On the other hand, interleukin-10 (IL-10) signaling not only plays a critical role in the metabolic

programming of macrophages towards the anti-inflammatory M2 phenotype countering LPS-induced downstream signals [16] but is also essential in the maintenance of intestinal homeostasis and barrier integrity [17]. Interestingly, much of IL-10's anti-inflammatory effects appear to be mediated by its downstream target, the signal transducer and activator of transcription-3 (STAT3) [18].

Peroxisome proliferator-activated receptors (PPARs) with its three isoforms, PPAR- $\alpha$ , PPAR- $\gamma$ , and PPAR- $\delta$ , are a group of nuclear receptors that regulate diverse metabolic and inflammatory processes, many of which are intimately linked to NASH [19]. That being the case and given the complex multifaceted nature of NASH, dual and pan PPAR agonists have recently evolved as multimodal candidates that are thought to open a new *vista* in NASH pharmacotherapy. PPAR- $\alpha$  is highly expressed in the liver and conveys the hypolipidemic effects of their well-known ligands, fibrates. Activation of PPAR- $\delta$ , on the other hand, stimulates  $\beta$ -oxidation in metabolically active tissues such as the liver, adipose tissue, and muscles [19]. Moreover, burgeoning evidence reveals that the polarization status of macrophages entails metabolic reprogramming to better support their specialized function [20]. As such, polarization of Kupffer cells and adipose tissue macrophages under the influence of PPAR activation was previously addressed in a NASH setting [21]. Interestingly, genome-wide association studies have also revealed the widespread expression pattern of these receptors in the gut tissue [22]. Both, PPAR- $\alpha$  [23] and  $\delta$  [24] have been shown to maintain intestinal homeostasis, albeit in a different context and by several mechanisms.

Accordingly, the current study sought to investigate whether elafibranor (ELA), a PPAR- $\alpha/\delta$  dual agonist, can modulate the polarization status of ileal macrophages towards restoring intestinal barrier integrity and reflecting onto the hepatic histological landscape in a NASH setting. Mechanistic insights on whether these effects are allied with a crosstalk between hepatic NF- $\kappa$ B and ileal IL-10/STAT3 signaling orchestrated by TLR4 were also provided.

## 2. Material and methods

### 2.1. *In vitro* investigations

#### 2.1.1. Cell culture

HepG2 cells were obtained from American Type Culture Collection (ATCC; VA, USA) and cultured using Dulbecco's Modified Eagle Medium (DMEM; Gibco, Life Technologies, Waltham, MA, USA) supplemented with 10% fetal bovine serum (FBS; Gibco, Life Technologies, Waltham,



MA, USA) and 1% of antibiotic-antimycotic solution (Gibco, Life Technologies, Waltham, MA, USA). Cells were maintained in a humidified incubator (Heracell™ VIOS 160i Tri-Gas CO<sub>2</sub> Incubator, 165 L; Thermo Fisher Scientific, Waltham, MA, USA) at 5% CO<sub>2</sub> and 37 °C and split when reaching approximately 70–80% confluence.

### 2.1.2. Induction and evaluation of steatosis *in vitro*

HepG2 cells were seeded in 6-well plates at a density of  $5 \times 10^5$  using FBS supplemented DMEM. The next day, cells were treated with either 10 μM elafibranor (ELA; BOC Sciences, NY, USA, CAS# 923978–27–2) dissolved in dimethyl sulfoxide (DMSO; Fisher Scientific, New Hampshire, USA; CAS#: 67–68–5) or its equivalent volume for positive and negative controls. Steatosis was induced on the third day, as described by a previous report [25]. Briefly, a freshly prepared free fatty acid (FFA)/bovine serum albumin (BSA; MP Biomedicals, Santa Ana, CA, USA; CAS#: 9048–46–8) conjugate was added to the wells with a final concentration of 0.5 mM FFA mixture of oleic acid (OA; Alfa Aesar, MA, USA; CAS#: 112–80–1) and palmitic acid (PA; Acros Organics, NJ, USA; CAS#: 57–10–3) in a ratio of 2:1, or an equivalent volume of FFA-free BSA for negative controls and incubated for 24 h. To evaluate fat accumulation, cells were either harvested for estimation of triglycerides (TG) and protein contents or fixed with 10% formalin for Oil Red-O staining. TG content was measured using Triglycerides GPO-PAP-enzymatic Colorimetric Assay Kit (Spectrum Diagnostics, Egypt, Ref-314) and normalized to protein content estimated using Pierce™ BCA Protein Assay Kit (Thermo Fisher Scientific, USA) following the respective manufacturers' instructions. Morphometric assessment of fat accumulation was carried out on Oil Red-O stained cells as described earlier [25] using ImageJ software (NIH, USA). *In vitro* experimental design is illustrated in Fig. 1A.

## 2.2. *In vivo* investigations

### 2.2.1. Animal model

Male C57BL/6 mice, weighing 25–35 gm, were obtained from Theodor Bilharz Research Institute, Giza, Egypt and inbred in the animal house facility of the Faculty of Pharmacy, The British University in Egypt. A combined model of dietary NASH and chronic colitis was adopted in the present study, as described by Gäbele et al. [26] with modification. Male littermates were randomly allocated into 3 experimental groups, namely, normal, HFD/DSS, and HFD/DSS+ELA. The normal group received a standard chow diet while the HFD/DSS and HFD/DSS+ELA groups received a high fat diet (HFD) [27] and 0.5% dextran sodium sulfate (DSS; MW ~40 kDa, TdB Consultancy AB, Uppsala, Sweden, CAS#: 9011–18–1) in drinking water. DSS was applied in cycles throughout the experimental period of 12 weeks, each cycle consisted of 7 days of DSS administration in drinking water and 10 days of DSS-free water. Additionally, HFD/DSS+ELA group received daily oral gavage with ELA at a dose of 30 mg/kg/day [28] in 1% tween 80 initiated after 8 weeks of induction for a duration of 4 weeks (Fig. 1B). In this model, DSS was used to experimentally simulate the clinical presentation of NASH patients with gut barrier dysfunction. Although primarily used in colitis models, DSS-induced disruptions are not confined to the colon, however, it also extends to include different regions of the small intestine [29,30]. And since the immunological milieu in the ileum, rather than the colon, distinctly dictates the intestinal barrier function and dysfunction [31], investigations of the current study were pursued on ileal tissues. Colonic tissues were only subjected to histopathological examination to confirm the DSS-induced colonic insults, being the primary site of its action. Throughout the experimental protocol, mice were housed in the animal house facility under constant conditions of temperature ( $23 \pm 2$  °C), humidity ( $50 \pm 10\%$ ), light/dark cycles (12 h/12 h) and allowed free access to drinking water. All experimental procedures were carried out in accordance with the EU Directive 2010/63/EU for animal experiments and were approved by the Ethical Committee of the Faculty of Pharmacy, The British

University in Egypt (EX-1902).

### 2.2.2. Sample collection and preparation

Twenty-four hours after the last ELA dose, mice were subjected to brief anesthesia and blood samples were withdrawn from the retro-orbital sinus for further fluorescein isothiocyanate (FITC)-dextran assay and estimation of lipopolysaccharide-binding protein (LBP) in serum. Liver, ileum, and colon tissues were also collected. For serum separation, blood samples were allowed to clot at room temperature for 30 min followed by centrifugation at 3000 RPM for 15 min. Meanwhile, tissue samples were either fixed in 10% formalin solution for histopathological and immunohistochemical analyses or flash-frozen using liquid nitrogen for gene expression and protein quantification assays. Tissue homogenates were prepared in PBS as 10% weight/volume. Protein content was determined in tissue homogenates using Pierce™ BCA Protein Assay Kit (Thermo Fisher Scientific, USA) following the manufacturer's instructions. In ELISA assays, concentration estimates in samples were then normalized to their respective protein content.

### 2.2.3. FITC-dextran intestinal permeability assay

In FITC-dextran permeability assay, mice are orally administered dextran as an LPS surrogate that follows its distribution kinetics but is instead conjugated to a fluorophore that permits its detection. If the gut barrier is intact, the large molecular size of FITC-dextran prevents it from passing through and, therefore, will not reach the systemic circulation whereas in a compromised barrier, leaked FITC-dextran becomes detected in serum and its concentration is proportional to the extent of barrier dysfunction. In the present study, 24 hrs after the last dose of ELA, FITC-dextran test for intestinal permeability was performed (Fig. 1C), as described by Volynets et al. [32]. Briefly, mice were transferred to clean cages with no bedding and a raised mesh to limit coprophagy. The following day, mice were challenged with a four-hour food deprivation period with free access to water. Subsequently, mice were administered oral gavage of 100 μl of FITC-dextran (TdB Consultancy AB, Uppsala, Sweden) at a concentration of 80 mg/ml in sterile PBS and four hours later, blood samples were drawn to extrapolate FITC concentrations from a standard curve *via* measuring the fluorescence using a CLARIOstar microplate reader (BMG Labtech MARS 3.32, Germany).

### 2.2.4. Estimation of lipopolysaccharide-binding protein in serum

LBP was estimated in serum samples using Mouse LBP ELISA Kit Picokine© (Boster Biological Technology, CA, USA, CAT#: EK1274) following the manufacturer's instructions.

### 2.2.5. Histopathological investigation of liver, ileum, and colon tissues

Formalin-fixed liver, ileal, and colon tissues were dehydrated in ascending alcohol grades before washing with xylene. Dehydrated tissues were then embedded in paraffin. Subsequently, tissues were cut into 4 μm thick sections using a microtome (microTEC, Duisburg, Germany) and then stained using hematoxylin and eosin (H&E). For each tissue type, ten random fields per section per animal were blindly examined at a magnification power of x200 using a light microscope (Zeiss, Oberkochen, Germany).

Liver sections were graded according to the following criteria for steatosis [33]:

Mild = 5–30%, moderate = 30–60%, and severe > 60% of hepatocytes affected.

### 2.2.6. Estimation of hepatic TLR4 and ileal iNOS and Arg1 gene expression

Total RNA was isolated from tissue samples using Direct-zol RNA Miniprep Plus kit (Zymoresearch Corp, USA, Cat#: R2072), according to the manufacturer's instructions. Extracted RNA quantity and quality were assessed using the Q5000 UV-Vis Nanodrop (Quawell, USA) by estimating the A260/A280 ratio. Reverse transcription was conducted using SuperScript IV One-Step RT-PCR kit (Thermo Fisher Scientific,

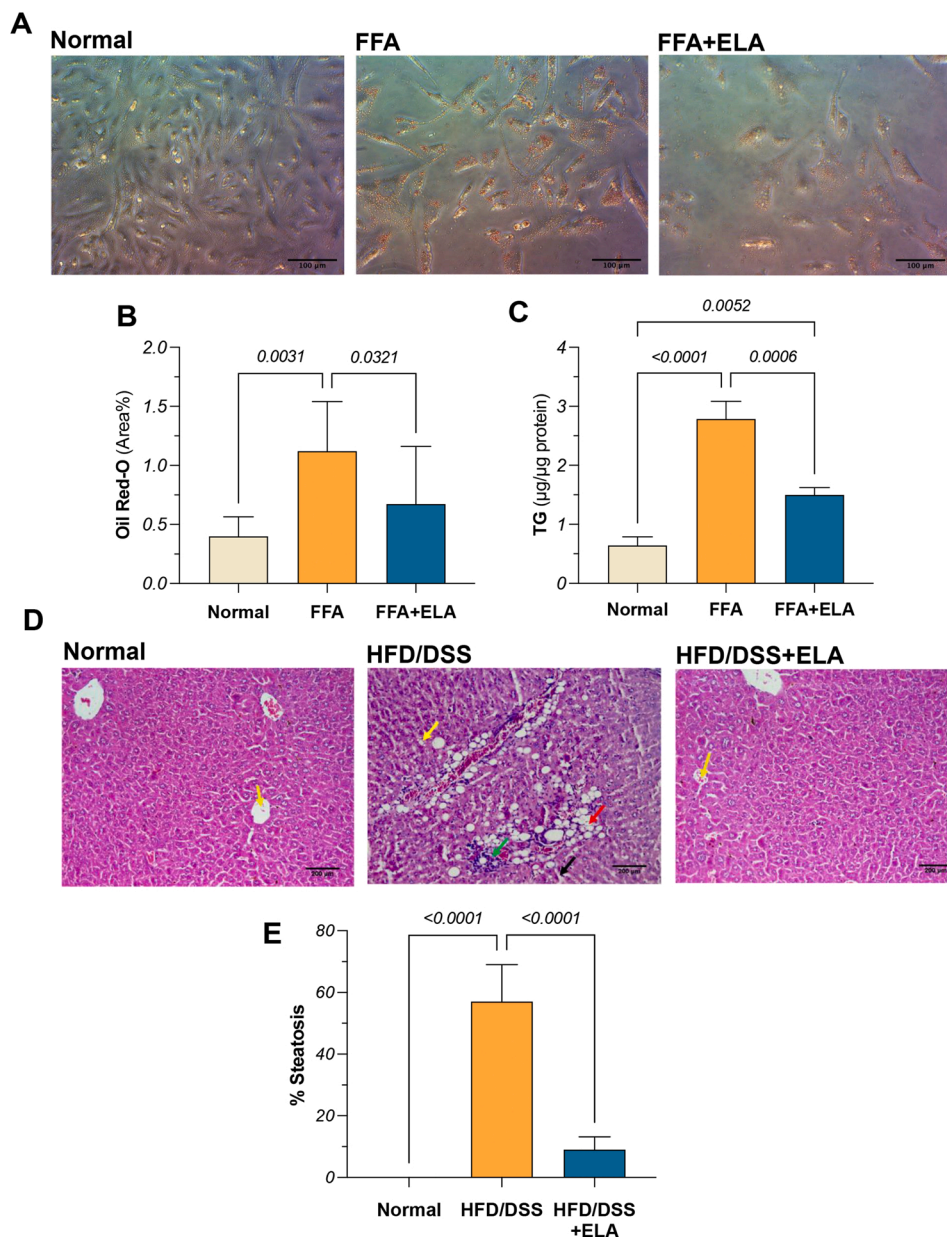


**Fig. 2.** Effect of ELA on free fatty acid (FFA)-induced lipid accumulation *in vitro* and histopathological hepatic alterations *in vivo*. (A) Representative images of Oil Red-O staining (ORO, x40) in FFA challenged-HepG2 cells with or without ELA treatment (10 μM) along with their corresponding (B) analysis of ORO staining area percentages, and (C) intracellular triglyceride (TG) content. (D) Hematoxylin and eosin (H&E, x200)-stained liver sections in normal, HFD/DSS, and HFD/DSS+ELA groups along with (E) steatosis scores. Statistical difference was tested using one-way ANOVA, followed by Tukey's multiple comparison test and significance was inferred for  $P < 0.05$ . All results are presented as means  $\pm$  S.D. Yellow arrow: central vein in (Normal & HFD/DSS+ELA) and multiple small to medium-sized fat droplets in (HFD/DSS); red arrow: single large-sized fat droplet in (HFD/DSS); green arrow: lymphocytic infiltrates in (HFD/DSS); black arrow: dilated congested sinusoid in (HFD/DSS).

Waltham, MA, USA, cat# 12594100), according to the manufacturer's recommendations followed by the polymerase chain reaction that was run on the 48-well StepOne platform (Applied Biosystems, USA). The following primers were used for TLR4 (NCBI accession no. NM\_021297.3): forward: 5'-CGCTTTCACCTCTGCCTTCACTACAG-3'; reverse: 5'-ACACTACCACAATAACCTTCCGGCTC-3', iNOS (NCBI accession no. NM\_010927): forward: 5'-GAGACAGGGAAGTCTGAAGCAC-3'; reverse: 5'-CCAGCAGTAGTTGCTCTCTTC-3'; Arginase-1 (Arg1) (NCBI accession no. NM\_007482): forward: 5'-CATTGGCTTGCAGACGTA-GAC-3'; reverse: 5'-GCTGAAGGTCTCTCCATCACC-3', and Glyceraldehyde 3-phosphate dehydrogenase (GAPDH) gene (NCBI accession no. NM\_008084.3): forward: 5'-CGTCCCCTAGACAAAATGGT-3'; reverse: 5'-TCAATGAAGGGTCTGTTGAT-3'. Fold change in gene expression was determined using delta-delta cycle threshold calculation ( $\Delta\Delta Ct$ ) and GAPDH was used as the endogenous normalization control [34].

#### 2.2.7. Estimation of hepatic inflammatory markers, NF- $\kappa$ B and I $\kappa$ B- $\alpha$

Phosphorylated nuclear factor kappa B [Ser536] (p-NF- $\kappa$ B, Cell Signaling Technology, USA, CAT#: 7173) and phosphorylated inhibitor

of kappa B-alpha [Ser32] (p-I $\kappa$ B $\alpha$ , Cell Signaling Technology, USA, CAT#: 7355) were estimated in hepatic tissue homogenates using ELISA following the manufacturer's instructions.

#### 2.2.8. Estimation of tight junctional proteins, claudin-1 and occludin, along with TLR4, IL-10, and macrophage polarization markers, iNOS and Arg1, in ileum

Avidin-biotin-immunoperoxidase technique was used for immunohistochemistry [35]. Primary monoclonal antibodies were used for claudin-1 (Invitrogen, MA, USA, CAT#: 37-4900), occludin (Invitrogen, MA, USA, CAT#: 33-1500), TLR4 (Santa Cruz Biotechnology, Inc., Santa Cruz, USA, CAT#: sc-293072), IL-10 (Santa Cruz Biotechnology, Inc., Santa Cruz, USA, CAT#: sc-8438), iNOS (Cell Signaling, MA, USA, CAT#: 13120), and Arg1 (Cell Signaling, MA, USA, CAT#: 43933) following a dilution of 1:100. For further colorimetric detection, streptavidin-biotin-peroxidase preformed complex and peroxidase-3,3'-diaminobenzidine were used complying with the manufacturer's instructions (Dako, Denmark). Mayer's hematoxylin was used for counterstaining. Expression percentages were then estimated in ten random

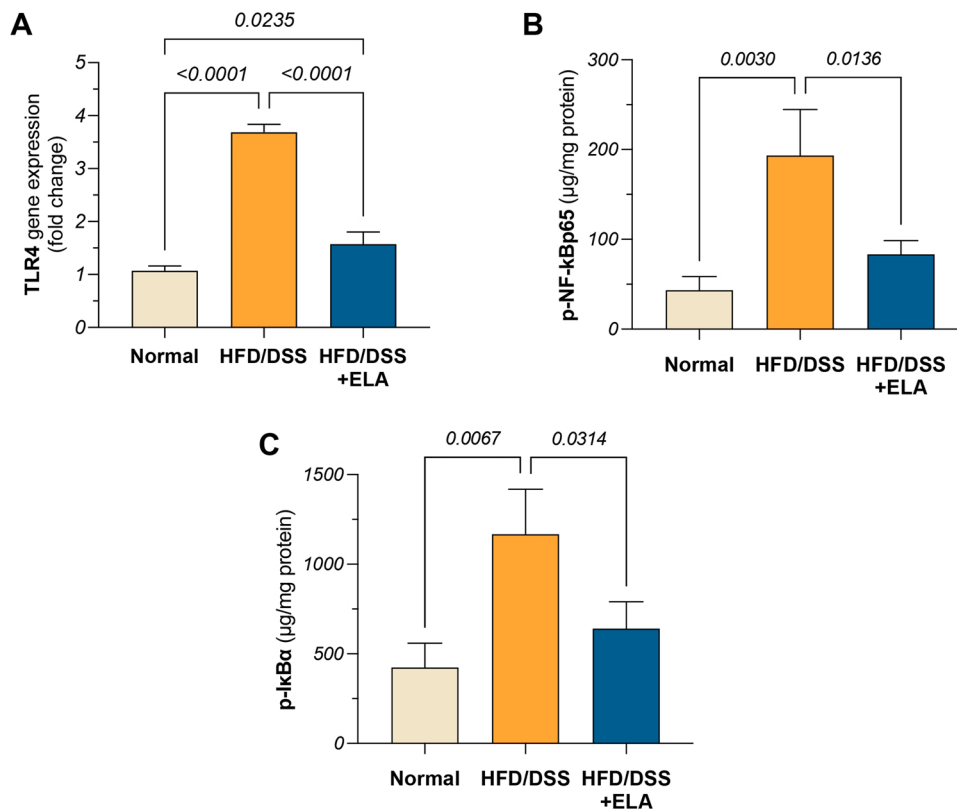


**Fig. 3.** Effect of ELA on hepatic TLR4/p-NF-κB/p-IκBα signaling. (A) TLR4 gene expression and (B) p-NF-κB and (C) p-IκBα protein levels in different groups. TLR4 relative gene expression is expressed as fold change from normal and was determined by qRT-PCR technique using delta-delta Ct ( $\Delta\Delta Ct$ ) following normalization to the housekeeping GAPDH gene. Protein levels of p-NF-κB and p-IκBα were estimated using ELISA. Statistical difference was tested using one-way ANOVA, followed by Tukey's multiple comparison test and significance was inferred for  $P < 0.05$ . All results are presented as means  $\pm$  S.D.

fields/section for each animal.

### 2.2.9. Estimation of $IFN\gamma$ and p-STAT3/t-STAT3 ratio in ileum

The following parameters were estimated in ileal tissue homogenates using ELISA:  $IFN\gamma$  (Proteintech, Rosemont, IL, USA, CAT#: KE10001) as well as phosphorylated and total levels of signal transducer and activator of transcription-3 (p-STAT3/t-STAT3, Abcam, Waltham, MA, USA, CAT#: ab176666) following the manufacturers' instructions.

### 2.3. Statistical analysis

Statistical analysis was performed using GraphPad Prism V 9.0 (GraphPad Software, Inc., San Diego, CA, USA). Statistical difference among groups was tested using one-way ANOVA, followed by Tukey's multiple comparison test and significance was inferred for  $P$  values below 0.05. All data are presented as means  $\pm$  standard deviation (S.D.).

## 3. Results

### 3.1. ELA decreased FFA-induced lipid accumulation in vitro

The capacity of ELA to affect hepatic lipid accumulation was examined in FFA-challenged HepG2 cells and is shown in Fig. 2A & 2B. FFA-challenged cells elicited a 3 folds surge in area % staining of Oil Red-O compared to BSA-treated normal counterparts ( $P = 0.0031$ ). Treatment with ELA, on the other hand, caused 40% reduction in the estimated area %, as compared to the FFA group ( $P = 0.0329$ ). Furthermore, incubation of ELA, 24 h prior to induction with FFA mixture, resulted in 46.29% reduction in TG accumulation compared to FFA-treated cells ( $P = 0.0006$ ) (Fig. 2C).

### 3.2. ELA countervailed hepatic NASH hallmarks

As shown in Fig. 2D, H&E-stained liver sections of normal mice

showed normal hepatic architecture with hepatocytes arranged in thin plates displaying normal cellular structure devoid of any fat deposits. Additionally, liver sinusoids and portal area showed no congestion and no lymphocytic infiltration, respectively. Meanwhile, H&E staining of HFD/DSS livers showed several derangements in hepatic architecture reminiscent of NASH, including multiple fat deposits, hepatocellular ballooning demonstrated as swollen hepatocytes with rarefaction of the cytoplasm, congested sinusoids as well as peri- and intra-portal lymphocytic infiltrates, whereas these transgressions were not found in liver sections of ELA-treated mice. Additionally, steatosis scores of HFD/DSS liver sections showed a mean steatosis score of 57%, while ELA-treated group showed a reduction in the mean steatosis score reaching 84%, as compared to HFD/DSS group ( $P < 0.0001$ ) (Fig. 2E).

### 3.3. ELA suppressed hepatic pro-inflammatory TLR4/NF-κB/IκBα signaling axis

Since bacterial products that breach the gut barrier are known to provoke an immune response in the hepatic tissue and drive NASH progression [4], we herein sought to substantiate this sequence of events starting from hepatic TLR4 that gets activated triggering downstream phosphorylation and nuclear translocation of p-NF-κB to ultimately upregulate several inflammatory genes. As shown in Fig. 3A, an upregulation of hepatic TLR4 gene expression was observed in the HFD/DSS group showing more than 3 folds surge ( $P < 0.0001$ ) from normal levels. The augmented TLR4 activity was accompanied by a significant elevation in the protein levels of both p-NF-κB and p-IκBα reaching 4.8 ( $P = 0.003$ ) and 2.8 ( $P = 0.0067$ ) folds, respectively, as compared to the normal group (Fig. 3B & 3C). On the other hand, hepatic TLR4 gene expression was curtailed to less than half of its expression ( $P < 0.0001$ ) in the ELA-treated group compared to the HFD/DSS group. Moreover, hepatic p-NF-κB and p-IκBα levels were also curbed by ELA showing a reduction by 56.89% ( $P = 0.0136$ ) and 45.14% ( $P = 0.0315$ ), respectively, compared to HFD/DSS group.



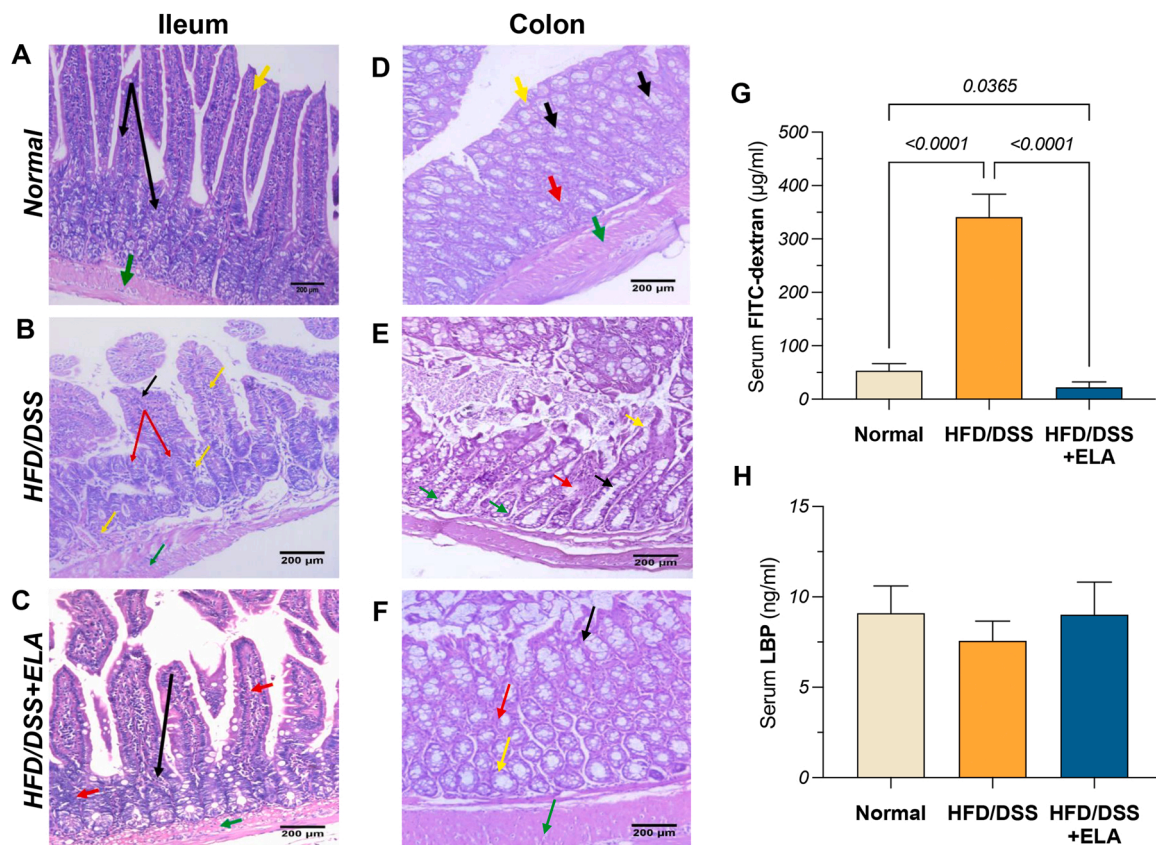


**Fig. 4.** Effect of ELA on histopathological alterations in ileum and colon along with serum FITC-dextran and LBP levels. Representative photomicrographs (x200) of H&E-stained (A-C) ileal and (D-F) colon sections from normal, HFD/DSS, and HFD/DSS+ELA groups. Serum levels of (G) FITC-dextran and (H) LBP in different groups. Serum FITC-dextran was detected using a spectrofluorometer while LBP was detected using ELISA. Statistical difference was tested using one-way ANOVA, followed by Tukey's multiple comparison test and significance was inferred for  $P < 0.05$ . All results are presented as means  $\pm$  S.D. *Black arrow*: villi to crypt ratio in (A & C), ulcerated villi in (B), and normal goblet cells in (D); *yellow arrow*: normal mucosal lining in (A & D), moderate infiltration of inflammatory cells in the mucosal and submucosal layers in (B), ulcerated epithelium in (E), and moderate inflammatory cells infiltrate in the mucosa in (F); *red arrow*: distorted villi to crypt ratio and partial loss of goblet cells in (B) and mild inflammatory infiltrates in (C); *submucosa* in (D), complete and mild loss of goblet cells in (E & F, respectively); *green arrow*: muscle layer (A-C, D & F) and inflammatory cell infiltration in mucosa and submucosa in (E).

### 3.4. ELA ameliorated histopathological alterations in ileum and colon

As demonstrated in Fig. 4A, ileal sections of the normal group showed an intact mucosal layer lined with mucin-secreting columnar cells with preserved villi to crypt ratio. Meanwhile, ileal sections from HFD/DSS mice showed marked ulceration of villi that was coupled with moderate inflammatory infiltrates in the mucosal and submucosal layers (Fig. 4B). Moreover, the same ileal sections showed atrophic mucosa with partial loss of goblet cells and distorted villi to crypt ratio. On the other hand, ileal sections from HFD/DSS+ELA group, showed preserved mucosal architecture with milder loss of goblet cells alongside fewer immune cell infiltrates in the mucosal layer and almost complete restoration of villi to crypt ratio (Fig. 4C). A similar pattern was observed in histopathological studies conducted in the colon where sections from normal mice (Fig. 4D) showed intact mucosal layer lined with mucin secreting columnar cells with preserved goblet cells. Meanwhile, colon sections from HFD/DSS mice showed distorted mucosal architecture. Mucosal and submucosal layers showed marked inflammatory cell infiltration while the surface epithelium showed significant ulceration resulting in hyperplasia (Fig. 4E). On the other hand, colon sections from HFD/DSS+ELA mice showed milder loss of goblet cells and fewer inflammatory cells infiltrating the mucosa and submucosa (Fig. 4F).

### 3.5. ELA decreased intestinal permeability

To evaluate gut barrier integrity, intestinal permeability was assessed via determining serum levels of FITC-dextran. As demonstrated in Fig. 4G, the HFD/DSS group showed an increase in serum FITC-dextran by 6.4 folds, as compared to the normal group ( $P < 0.0001$ ). Treatment with ELA, on the other hand, caused a significant reduction in FITC-dextran serum levels reaching almost 93% ( $P < 0.0001$ ).

### 3.6. Neither HFD/DSS nor ELA altered serum LBP levels

LBP is a protein that is produced by the liver and secreted into the circulation to sequester the available LPS pool. As shown in Fig. 4H, no significant difference was reported in serum LBP levels across groups which may indicate that LBP might not be altered in the currently adopted experimental conditions.

### 3.7. ELA restored normal tight junction protein expression in ileum

To further validate alterations in intestinal barrier integrity, ileal immunoreactivity of tight junction proteins, claudin-1 and occludin, was estimated. The HFD/DSS group showed an 80% reduction in claudin-1 expression levels compared to normal ( $P = 0.0259$ ) while treatment with ELA resulted in a surged expression reaching 7.5 folds, as compared to the HFD/DSS group ( $P = 0.0008$ ), with no significant change relative to normal (Figs. 5A-C and 5G). Occludin immunoreactivity, on the other

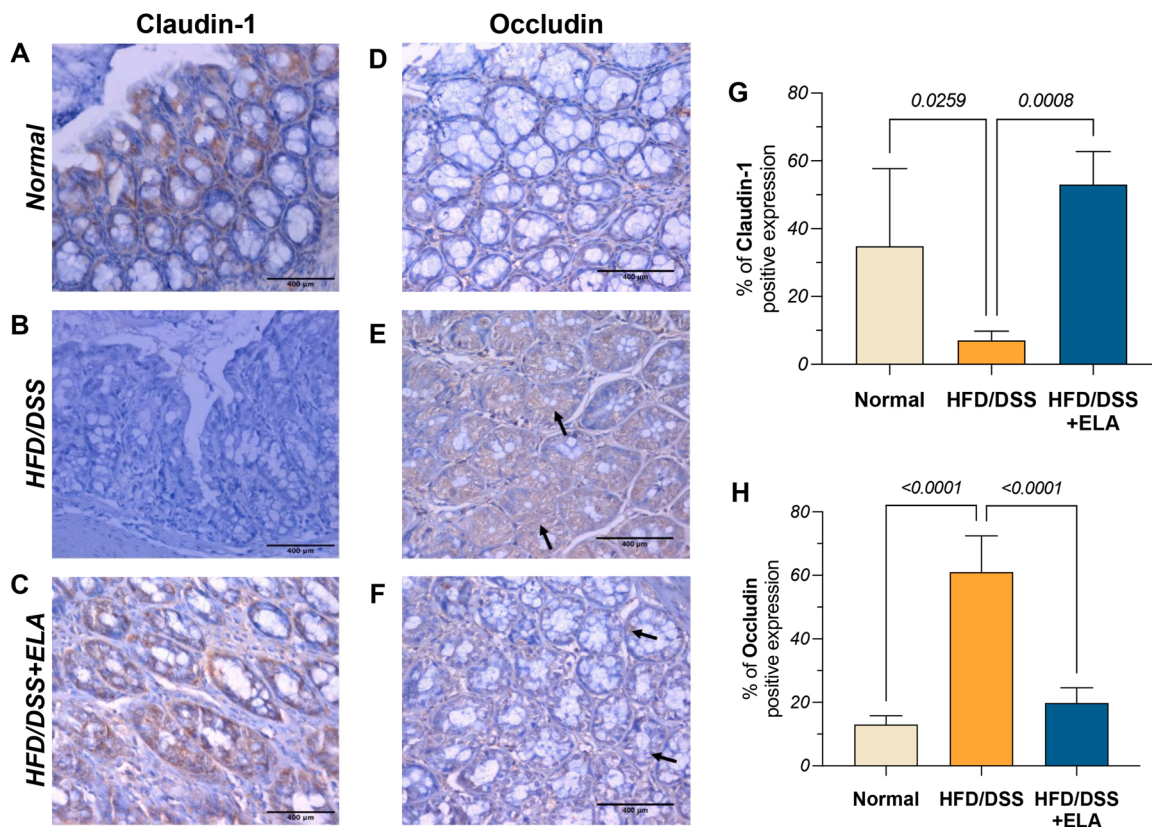


**Fig. 5.** Effect of ELA on claudin-1 and occludin tight junction proteins expression. Representative photomicrographs (DAB, x400) of ileal sections from normal, HFD/DSS, and HFD/DSS+ELA groups against (A-C) claudin-1 and (D-F) occludin. Semi-quantitative analyses for stained sections representing the percentage of positive expression of (G) claudin-1 and (H) occludin in different groups. Statistical difference was tested using one-way ANOVA, followed by Tukey’s multiple comparison test and significance was inferred for  $P < 0.05$ . All results are presented as means  $\pm$  S.D.

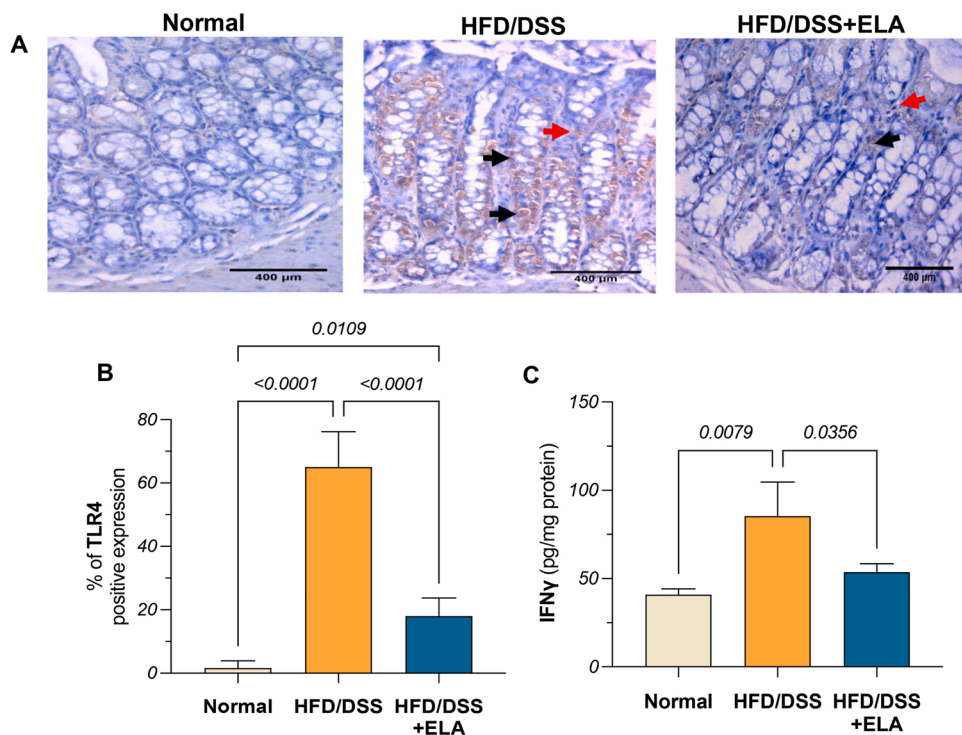


**Fig. 6.** Effect of ELA on pro-inflammatory M1 polarizing signals, TLR4 and IFN $\gamma$ , in ileum. (A) Representative photomicrographs (DAB, x400) and the subsequent (B) semi-quantitative analysis for TLR4 positive expression in ileal sections from normal, HFD/DSS, and HFD/DSS+ELA groups. (C) IFN $\gamma$  levels in ileal tissue homogenates from different groups estimated using ELISA. Statistical difference was tested using one-way ANOVA, followed by Tukey’s multiple comparison test and significance was inferred for  $P < 0.05$ . All results are presented as means  $\pm$  S.D.



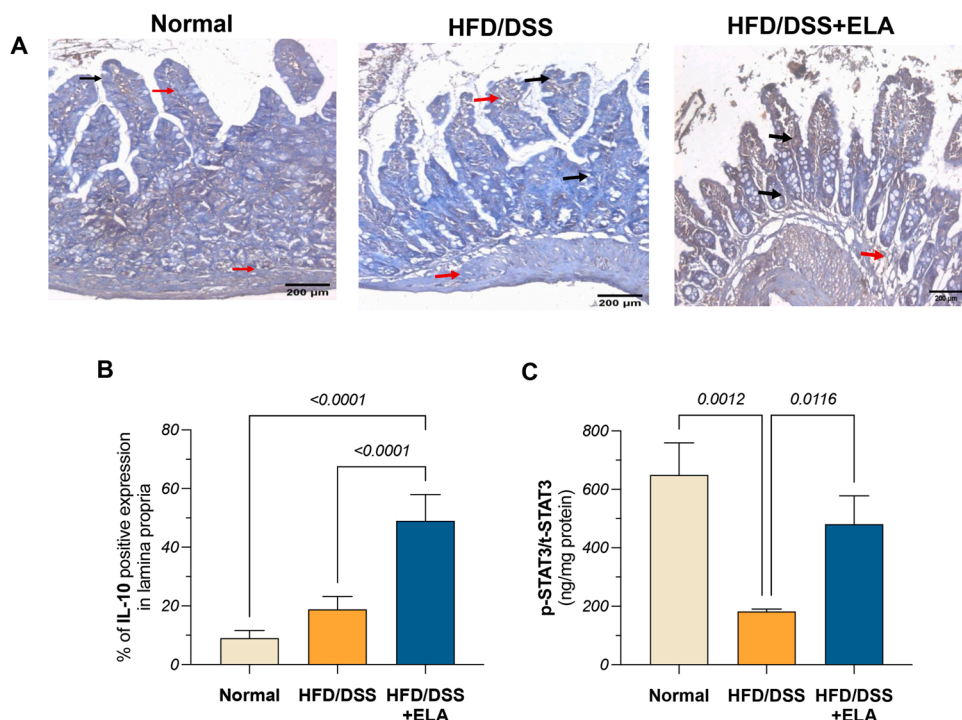


**Fig. 7.** Effect of ELA on M2-polarizing IL-10 and its downstream STAT3 signaling in ileum. (A) Representative photomicrographs (DAB, x400) and the subsequent (B) semi-quantitative analysis for IL-10 positive expression in normal, HFD/DSS, and HFD/DSS+ELA groups. (C) p-STAT3/t-STAT3 levels in ileal tissue homogenates from different groups estimated using ELISA. Statistical difference was tested using one-way ANOVA, followed by Tukey's multiple comparison test and significance was inferred for  $P < 0.05$ . All results are presented as means  $\pm$  S.D.

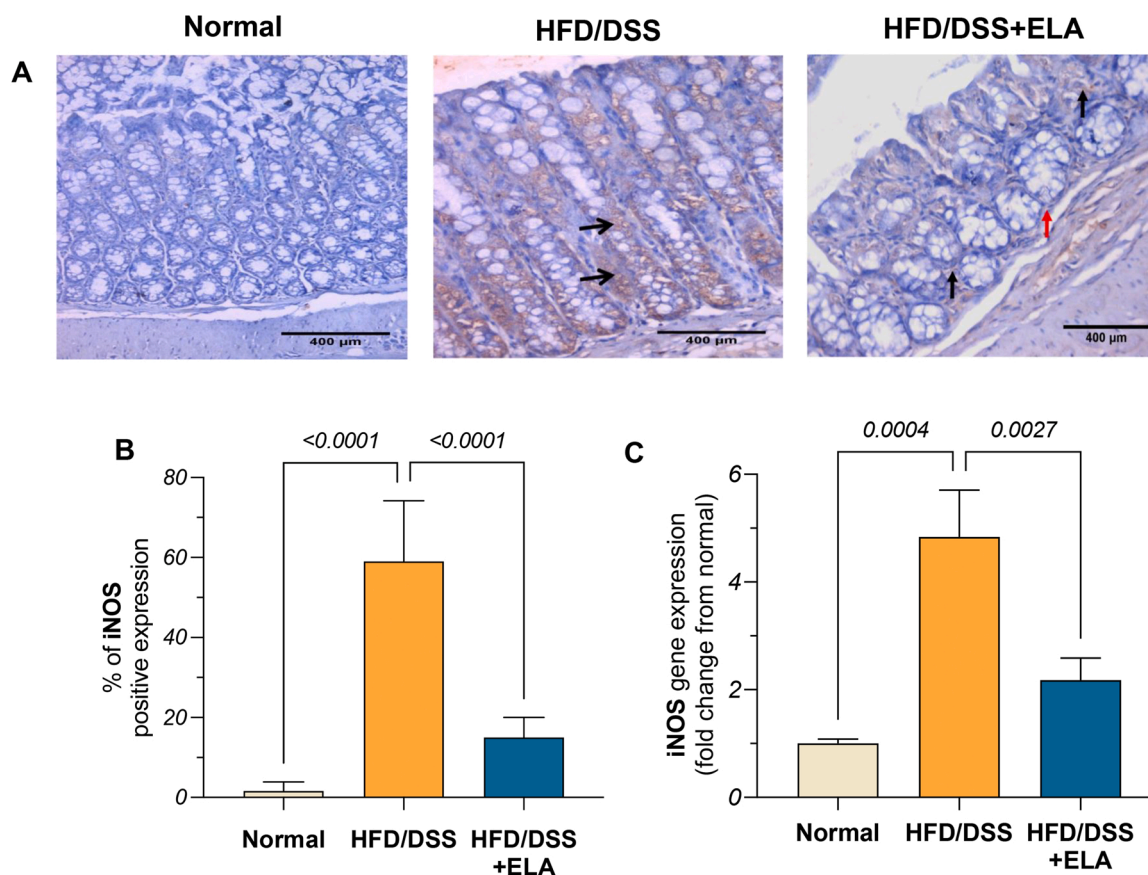


**Fig. 8.** Effect of ELA on iNOS as an M1 polarization marker. (A) Representative photomicrographs (DAB, x400) and the subsequent (B) semi-quantitative analysis for ileal iNOS positive expression in normal, HFD/DSS, and HFD/DSS+ELA groups. (C) Relative gene expression analysis of iNOS. Relative gene expression in (C) is expressed as fold change from normal and was determined by qRT-PCR technique using delta-delta Ct ( $\Delta\Delta Ct$ ) following normalization to the housekeeping GAPDH gene. Statistical difference was tested using one-way ANOVA, followed by Tukey's multiple comparison test and significance was inferred for  $P < 0.05$ . All results are presented as means  $\pm$  S.D.

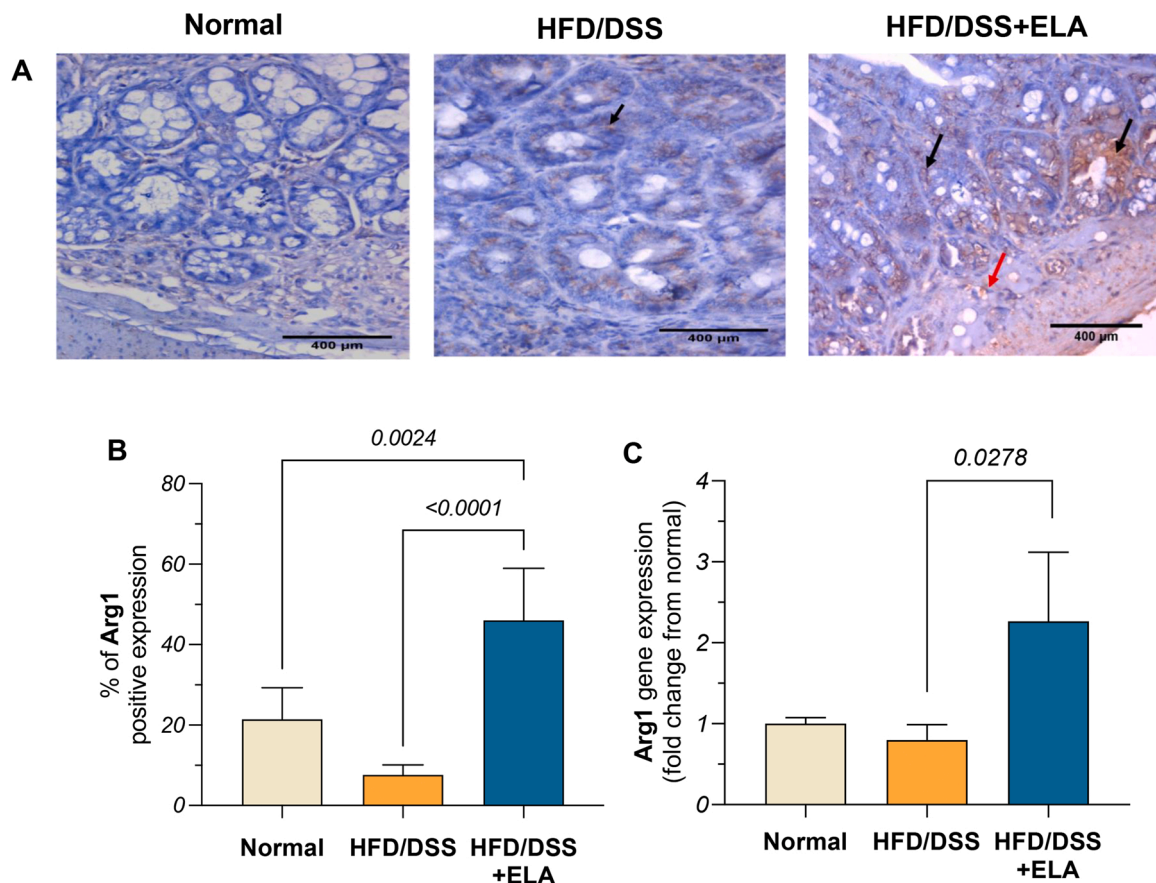


**Fig. 9.** Effect of ELA on Arg1 as an M2 polarization marker. (A) Representative photomicrographs (DAB, x400) and the subsequent (B) semi-quantitative analysis for ileal Arg1 positive expression in normal, HFD/DSS, and HFD/DSS+ELA groups. (C) Relative gene expression analysis of Arg1. Relative gene expression in (C) is expressed as fold change from normal and was determined by qRT-PCR technique using delta-delta Ct ( $\Delta\Delta Ct$ ) following normalization to the housekeeping GAPDH gene. Statistical difference was tested using one-way ANOVA, followed by Tukey's multiple comparison test and significance was inferred for  $P < 0.05$ . All results are presented as means  $\pm$  S.D.

hand, was higher in the HFD/DSS group by 24 folds compared to normal ( $P < 0.0001$ ), however, a 68% reduction was observed in the HFD/DSS+ELA, as compared to the HFD/DSS group ( $P < 0.0001$ ) (Figs. 5D-F and 5H). It is worth mentioning that for the HFD/DSS group, most of the occludin expression was cytoplasmic (Fig. 5E).

### 3.8. ELA modulated ileal milieu to suppress M1 polarizing signals, TLR4 and IFN $\gamma$

The polarization status of macrophages inhabiting the lamina propria markedly influences intestinal homeostasis and barrier integrity where M1 macrophages aggravate and M2 macrophages restrain intestinal insults. Two of the most potent well-established M1 polarizing signals were estimated in the ileum in the current study, namely, TLR4 and IFN $\gamma$ . Ileal tissue from the HFD/DSS group elicited a milieu supportive of M1 polarization characterized by augmented TLR4 immunoreactivity (Fig. 6A & 6B) as well as a significant increase in IFN $\gamma$  levels (Fig. 6C) reaching 40 folds ( $P < 0.0001$ ) and 2 folds ( $P = 0.0079$ ), respectively, as compared to the normal group. This was significantly curtailed upon treatment with ELA, with reductions reaching 72.31% ( $P < 0.0001$ ) and 37.15% ( $P = 0.0356$ ) in TLR4 ileal expression and IFN $\gamma$  levels, respectively, as compared to the HFD/DSS positive control group. These results might indicate that ELA was capable of dampening the inflammatory milieu in the ileum away from the pro-inflammatory M1 polarization.

### 3.9. ELA modulated ileal milieu to enhance M2 polarizing IL-10/STAT3 signaling

Since the gut tissue harbors the largest pool of IL-10-producing macrophage population in the body and given that both IL-10 and its downstream target, STAT3, were exhaustively linked to the maintenance of intestinal homeostasis, alterations in IL-10 and STAT3 were estimated in ileal tissues. Ileal IL-10 immunoreactivity elicited a 52% increase in the HFD/DSS group ( $P = 0.0565$ ), as compared to normal, while IL-10 levels of ELA-treated group surged 2.6 folds relative to the HFD/DSS group ( $P < 0.0001$ ) (Fig. 7A & 7B). Moreover, the ratio of p-STAT3/t-STAT3 in the HFD/DSS group showed a reduction reaching 72% compared to normal ( $P = 0.0012$ ), whereas ELA treatment resulted in almost 3 folds increased ratio when compared to HFD/DSS estimates ( $P = 0.0116$ ) (Fig. 7C).

### 3.10. ELA promoted M2 polarization in ileum

To validate MP secondary to ileal milieu alterations in polarizing signals, iNOS and Arg1 as functional markers of M1 and M2 phenotypes, respectively, were investigated. Regarding iNOS, the HFD/DSS group showed almost 5 folds ( $P = 0.0004$ ) and 37 folds ( $P < 0.0001$ ) increase in its ileal gene expression and immunoreactivity, respectively, as compared to normal. On the other hand, treatment with ELA caused 55% ( $P = 0.0027$ ) and 74.6% ( $P < 0.0001$ ) reductions in iNOS gene and immunohistochemical expression, respectively, as compared to HFD/DSS (Fig. 8 A-C). An opposite pattern was observed with the expression of Arg1, an M2 polarization marker, where HFD/DSS showed lower



expression levels reaching 64.5%, as compared to the normal group ( $P = 0.0719$ ), however, no change was observed in the relative gene expression levels among these two groups. Meanwhile, ELA treatment resulted in almost 3 folds ( $P = 0.0278$ ) and 6 folds ( $P < 0.0001$ ) upsurge in Arg1 gene expression and ileal immunoreactivity, respectively, as compared to the HFD/DSS group (Fig. 9 A-C). These results suggest a likely skewness towards the M1 and M2 phenotypes in the HFD/DSS and ELA-treated groups, respectively.

#### 4. Discussion

The pathogenesis of NASH is complex involving a myriad of metabolic and inflammatory insults that take place not just in the hepatic tissue, but also extrahepatically, and is in that sense considered a systemic disease [36]. Particularly, pathogenic processes in the gut leading to an impaired barrier function are implicated in NASH progression [4]. Macrophages are profound influencers of intestinal homeostasis, yet how exactly their polarization status contributes to barrier integrity and bacterial translocation in NASH has been little explored. PPARs are ligand-activated transcription factors belonging to the nuclear hormone receptor superfamily that are critical for maintaining metabolic homeostasis by sensing nutrients and modulating intracellular metabolism [19]. Accumulating evidence reinforces the notion that metabolic programming in macrophages lies at the center of their functional plasticity [20]. As such, PPAR activation was previously reported to fine-tune metabolism in macrophages, subsequently impinging on their polarization status [21]. Additionally, activation of different PPAR isoforms was found to confer protection against intestinal insults [23,24], yet limited studies have attempted to decipher the intricate molecular underpinning of how PPAR activation might potentially modulate compromised gut barrier integrity and impede bacterial translocation as critical pathological events implicated in NASH. This has prompted us to probe the potential role of dual PPAR  $\alpha/\delta$  activation using ELA on ileal MP in an experimentally induced NASH-colitis model. Alterations in the ileal IL-10/STAT3 signaling axis were investigated to gain further mechanistic insights into the underlying mechanisms driving MP, while the potential hepatic consequences of such phenotypic switching were explored by assessing TLR4/NF- $\kappa$ B/I $\kappa$ B $\alpha$  signaling in the liver.

Since several simultaneous mechanisms likely contribute to NASH progression, a promising drug candidate should address more than a single aspect of this complex disease [37]. As such, a proof-of-concept *in vitro* study was carried out in fat-laden HepG2 cells to elucidate the capacity of ELA in tackling the metabolic facet of NASH where a mitigation in TG levels and fat accumulation was observed in ELA-treated cells. These results are in accordance with the recent work conducted by Boeckmans and colleagues who showed that, compared to other PPAR agonists, ELA elicited the strongest anti-NASH properties *in vitro* [38].

TLR4 is a pattern recognition receptor that recognizes gut-derived LPS. Upon stimulation, TLR4 interacts with a cohort of adaptor proteins that ultimately lead to NF- $\kappa$ B activation [39]. At steady state, NF- $\kappa$ B is chained down to I $\kappa$ B $\alpha$ , the activation of which is under the tight control of the inhibitor of kappa-B kinase (IKK) complex formed of IKK- $\alpha$ , IKK- $\beta$ , and IKK- $\gamma$ . Upon upstream stimulation, phosphorylated IKK- $\beta$  catalyzes the phosphorylation of I $\kappa$ B $\alpha$ , thus releasing it off the NF- $\kappa$ B dimer, provoking nuclear translocation and its transcriptional activity [39]. Multiple lines of evidence implicate the activation of hepatic TLR4 and its downstream effector, NF- $\kappa$ B, in the pathogenesis of NASH [6,40,41]. TLR4 is ubiquitously expressed by hepatocytes, Kupffer cells, and hepatic stellate cells, the activation of which contributes to different pathogenic processes fueling NASH. NF- $\kappa$ B, on the other hand, is a transcriptional factor that controls the expression of multiple pro-inflammatory mediators implicated in NASH which was evident both experimentally [8] and clinically [10]. In the present study, hepatic TLR4 expression was found to be upregulated along with hepatic p-NF- $\kappa$ B/p-I $\kappa$ B $\alpha$  levels in the HFD/DSS mice, thus corroborating with the

previous findings. The surge in TLR4/NF- $\kappa$ B/p-I $\kappa$ B $\alpha$  signaling axis reported herein also aligns with recent clinical evidence where a similar pattern was observed in NASH biopsies compared to normal livers [39].

An intriguing interplay bridging metabolism to inflammation in the context of NAFLD can be viewed in the previously reported negative regulatory loop between TLR4 and PPAR- $\alpha$ . LPS-activated TLR4 was previously shown to negatively regulate hepatic PPAR- $\alpha$  expression [42], while PPAR- $\alpha$  deletion in primary hepatocytes resulted in the upregulation of TLR4 [43]. Intriguingly, in the present study, the activation of PPAR- $\alpha/\delta$  following ELA treatment curtailed hepatic TLR4 expression which was further confirmed by lower levels of p-NF- $\kappa$ B/p-I $\kappa$ B $\alpha$ . This goes in agreement with the aforementioned reports. Additionally, although gut-derived LPS is inherently recognized by TLR4, LPS is not the exclusive activator of the receptor, as saturated fatty acids were also reported to trigger its activation [44]. And since PPAR- $\alpha$  and - $\delta$  induce hepatic fatty acid oxidation [19] and reduce hepatic fat accumulation, as evident in the *in vitro* arm of the current study, the saturated fatty acid pool available for TLR4 stimulation is, therefore, diminished. Accordingly, hepatic TLR4 downregulation in the ELA-treated group can conservatively be attributed to either direct interaction with hepatic TLR4/p-NF- $\kappa$ B/p-I $\kappa$ B $\alpha$  signaling, or to reduced availability of its agonists whether it is the gut-derived LPS, due to barrier fortification, or reduced saturated fatty acid pool due to hepatic fatty acid oxidation induction.

Understanding the contribution of a compromised intestinal barrier in the progression of NAFLD towards NASH necessitates the dissection of the underlying local intestinal inflammatory events. Accordingly, the focus of the current study was shifted towards the gut front of the enterohepatic crosstalk, with particular emphasis on the contribution of innate immune responses to barrier integrity. Hence, factors that drive ileal MP, as well as implications of polarization factors and outputs, were also investigated herein, with the expression of key tight junction proteins, as the ultimate thread protecting the liver, lying front and center of our pondered research question. Therefore, we first sought to assess alterations in barrier integrity. Owing to the complexity of this barrier, such assessment begets the estimation of multiple indicators of integrity [45]. Accordingly, in the current study, histopathological investigations were first carried out in H&E-stained ileum and colon sections for qualitative characterization of barrier integrity, while serum LBP, FITC-dextran permeability assay and ileal immunoreactivity of tight junction proteins were carried out for quantitative assessment.

The findings reported herein depicted the capacity of ELA to alleviate barrier dysfunction that was histologically evident in H&E-stained ileum and colon sections, significant curtailment of systemic FITC-dextran levels, as well as normalization of ileal tight junction proteins expression. The present results are interesting owing to scarcity of evidence tying PPAR- $\alpha/\delta$  to barrier function. On the other hand, no significant changes were observed in serum LBP level across groups, which was also the case in our previous study [46]. One rationale that can be provided is the lack of temporal reliability of serum LBP levels as an indicator of barrier integrity. Indeed, LBP is an acute-phase protein biomarker best apt to capture changes in acute rather than chronic alterations in barrier function [47]. In the present study, LPS measurement was not sought based on several limitations this assay holds as previously reported by Munford RS [45,48]. These limitations are due to the heterogeneous nature of LPS which might compromise the reliability of the assay standards used in the detection kits, as each one includes its own LPS preparation method likely producing different dose-response curves. Accordingly, the estimated LPS in serum samples may not directly match that of the LPS used to standardize the assay.

The markers used in the current study in order to identify MP reflect their functional plasticity and their contribution to intestinal homeostasis [15,49]. Differential expression of iNOS and Arg1 markedly influences intestinal homeostasis where the former aggravates, and the latter attenuates the inflammatory tone of the intestinal tissue [50]. Thus, expression of these enzymes, while validating M1/M2

polarization, is functionally relevant to the maintenance of barrier integrity. This can also be implied by the prototypic signaling cues driving MP that were investigated in the current study. In fact, the homeostatic roles IL-10 plays in the maintenance of gut barrier [17] as well as the disruptive capacity of both TLR4 [51] and IFN $\gamma$  [52] have been reported in a number of settings.

One of the key players of inflammation-driven barrier disruption is the pattern recognition receptor, TLR4. Previous investigations employing either HFD [51] or DSS [53] indicated that intestinal TLR4 activation mediated barrier dysfunction and downregulated tight junction expression. Both PPAR isoforms, on the other hand, elicit some capacity to antagonize TLR4 actions, as discussed earlier with hepatic TLR4 [24,43]. TLR4 was not, however, linked to tight junction expression or intestinal permeability in these studies and the potential interplay tying PPAR-mediated actions to the gut barrier function was, heretofore, unexplored in a NASH setting. In concert with these studies, ileal TLR4 expression surged in the HFD/DSS group which correlated negatively with claudin-1 protein expression. Additionally, a significant downregulation of ileal TLR4 that was coupled with restored expression of the key tight junctional protein, claudin-1, downstream to PPAR  $\alpha/\delta$  dual activation was observed. Treatment with ELA resulted in the normalization of the ileal tight junction proteins, claudin-1 and occludin, which was evident by the insignificant difference observed when compared to the normal group. However, the pattern of tight junctions protein expression showed a discrepancy where claudin-1 levels were lowest and occludin levels were highest in ileal sections of the HFD/DSS control group. This opposite pattern could be explained by the notion that the expression of tight junction proteins does not necessarily imply their proper assembly towards a firmer barrier. Particularly, occludin and zonula occludens-1 expression were previously reported to surge in pathological settings in which barrier integrity is compromised [54,55] suggesting that claudin-1 is the backbone of tight junction strands [56]. Furthermore, ileal occludin expression in HFD/DSS group was predominantly localized in the cytoplasm, essentially away from the intestinal epithelial cell membrane to serve its barrier-fortifying function. The increase in the cytoplasmic expression also paralleled a similar increase in IFN $\gamma$  which was previously reported to result in phosphorylation and subsequent internalization of occludin [52].

Interferon-gamma (IFN $\gamma$ ), a prototypical pro-inflammatory cytokine, is heavily implicated in gut barrier disruption and is known to mediate this by provoking claudin-1 and occludin internalization [52]. Moreover, congruent lines of evidence suggests that IFN $\gamma$ -induced iNOS expression, at least partly, mediates such disruption [57]. Furthermore, activation of IFN $\gamma$  receptors upregulated TLR4 expression in cultured macrophages and both LPS and IFN $\gamma$  synergize for iNOS production [14]. As such, in the current study, we sought to estimate ileal IFN $\gamma$ , where the HFD/DSS group demonstrated a robust production in its level paralleling the increase in iNOS and claudin-1 curtailment, corroborating with the previously mentioned studies, whereas ELA decreased its ileal levels. This is likely a PPAR- $\alpha$  and - $\delta$  driven effect since the capacity of PPAR- $\alpha$  to confer protection against intestinal insults by suppressing IFN $\gamma$  levels was previously reported in a DSS-induced colitis model [23]. Moreover, PPAR- $\delta$  knockout mice were also shown to be more susceptible to DSS-induced colitis while expressing higher levels of intestinal IFN $\gamma$  [58].

IL-10 is an immunoregulatory cytokine critical in maintaining intestinal homeostasis [17]. The gut tissue harbors the largest pool of IL-10-producing macrophages in the body [59]. Mice with myeloid specific genetic defects in IL-10 [60], IL-10 receptor (IL-10R) [61], or its major downstream target, STAT3 [62], exhibit either spontaneous colitis or heightened inflammatory responses when challenged with DSS. Macrophages lacking IL-10R are markedly skewed towards the M1 pro-inflammatory phenotype *in vitro* [63]. This observation is also evident *in vivo* as seen in macrophages inhabiting the intestinal lamina propria [61] where defective IL-10R in myeloid cells was found to alter iNOS/Arg1 levels towards wreaking the intestinal barrier. In fact, IL-10's

capacity to counteract LPS-induced pro-inflammatory cytokine secretion was shown to be mediated through metabolic reprogramming of macrophages in better support of their immunosuppressive function, an effect reported to be STAT3-dependent [16,64]. Similarly, a cellular crosstalk between TLR4 and IL-10/STAT3 signaling towards intestinal homeostasis was previously reported [65]. Intriguingly, in the present study, IL-10 lamina propria levels tended to increase in HFD/DSS ileums while p-STAT3/t-STAT3 ratios subsided. The marginal increase in IL-10 levels might have been in response to the higher expression of lamina propria TLR4 observed in HFD/DSS ileums. TLR4 activation in macrophages not only results in the production of pro-inflammatory cytokines but in a delayed manner, stimulates the production of IL-10 for signal termination [59] in an attempt to restore homeostasis. However, the low p-STAT3/t-STAT3 ratio along with the only marginal increase in IL-10 suggest that signal strength might not have been powerful enough to subdue the augmented TLR4 and IFN- $\gamma$  responses. On the other hand, in the ELA-treated group, significant increase in IL-10 and restored p-STAT3/t-STAT3 ratio were observed.

In the current study, the HFD/DSS group demonstrated an increase in iNOS whereas ELA treatment resulted in an upsurge of Arg1. These effects were observed on both the gene and protein levels. Additionally, the protein levels of the M2 marker, CD206, were estimated by western blot where the ELA-treated group exhibited an increase in its level that failed to reach significance relative to the HFD/DSS group (data in [Supplementary Material](#)). The present findings are in accordance with previous studies showing a deleterious role for enhanced iNOS-mediated production of NO [15,66] highlighting the protective role of Arg1 in the maintenance of intestinal homeostasis [49]. The alterations in intestinal iNOS/Arg1 levels observed in the HFD/DSS controls with respect to barrier integrity in NASH are corroborated by a recent study, albeit in a different induction model while also lacking a focus on the potent M1 polarizing agents reported herein [50] which was also clinically validated by the same research group [67].

Robust engagement of the M1 program requires simultaneous activation of macrophages with LPS (TLR4/NF- $\kappa$ B) as well as IFN $\gamma$  [14]. In the present study, IFN $\gamma$  in HFD/DSS mice presented a similar behavior pattern to that of TLR4, thus further supporting potent stimulation of lamina propria macrophages towards the M1 phenotype. Interestingly, it has been reported that PPAR- $\alpha$  activation downregulates iNOS mRNA expression in LPS-triggered bone marrow-derived macrophages [68], augments iNOS degradation in a proteasome-dependent manner [69] as well as curbs NO production in RAW264.7, the macrophage cell line [70]. On the other hand, PPAR- $\delta$  activation drives macrophages to an M2-like anti-inflammatory phenotype in a STAT6-dependent manner, thereby upregulating Arg1 [71]. Simultaneous activation of PPAR- $\alpha/\delta$  using ELA in the present study, therefore, might have offered complementary effects that enhanced ileal M2 polarization and subsequently conferred protection of intestinal barrier integrity.

The current study holds several limitations. Whilst the inference is strengthened by several immunohistochemical estimations acknowledging the spatial distribution of markers and supporting the proposed mechanistic insights, the captured images are static. Particularly, markers were estimated at a single point in time (12 weeks), while inflammation is a spatiotemporal dynamic state that is a vibrant dance of cells tangoing one another, infiltrating and exiting the site of insult, fluctuating in phenotypes, and profoundly shaping one another [72]. Accordingly, this is one limitation that may defer the translatability of the outcome until further investigations vouch for it. Another possible caveat is relying heavily on iNOS and Arg1 as M1 and M2 polarization markers, respectively. Whereas these markers are indeed emblematic of distinct macrophage phenotypes, they have also been shown to be expressed by cells other than macrophages [73]. One limitation is also related to PPAR expression which is known to be disproportionate between mice and men. Indeed, PPAR- $\alpha$  is over-represented in mice compared to human hepatocytes, which might partly explain why the promising results displayed by fibrates, as PPAR- $\alpha$  activators, in murine

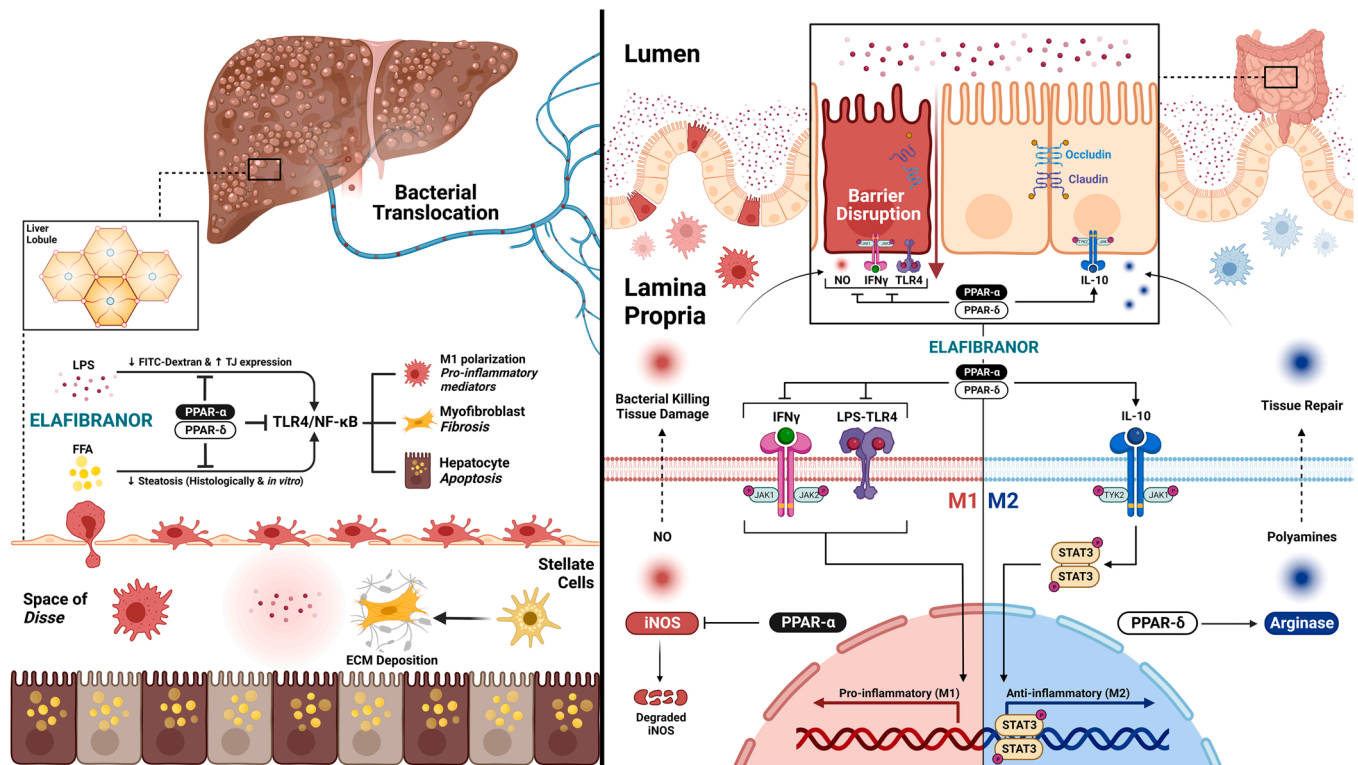


**Fig. 10.** Schematic illustration for the proposed modulatory roles of ELA on hepatic and ileal inflammatory insults in an HFD/DSS-induced NASH/colitis model. PPAR- $\alpha/\delta$  dual agonism by ELA suppresses pro-inflammatory hepatic TLR4/NF- $\kappa$ B activation secondary to barrier disruption. Once gut barrier integrity is disrupted, a feed-forward inflammatory loop is initiated in the lamina propria that polarizes macrophages towards the M1 phenotype. Triggered M1 lamina propria macrophages express iNOS and release the ileal pro-inflammatory cytokine, IFN $\gamma$ , that works in an autocrine/paracrine manner perpetuating the inflammatory milieu and further disrupting claudin-1 and occludin expression. Distinct and complementary actions of PPAR- $\alpha/\delta$  dual activation mitigate TLR4/IFN $\gamma$  and boost IL-10/STAT3 signaling subsequently skewing M2 macrophages that express Arg1 paving the way for tissue repair and barrier restoration. Created with BioRender.com.

models of NASH were lost in translation [74].

In conclusion, the current study highlights a key role of intestinal MP in the modulation of barrier integrity in NASH. A potential therapeutic response to ELA, the dual PPAR- $\alpha/\delta$  agonist, in a preclinical model of NASH emphasizing on the enterohepatic crosstalk, was also provided. Hence, the current study findings suggest a capacity of ELA towards alleviating barrier dysfunction, mitigating bacterial translocation, and reinforcing tight junction proteins through complementary activities on intestinal macrophages. The proposed effect of ELA in experimental NASH with gut barrier dysfunction is illustrated in Fig. 10. While failing to meet its promise in the RESOLVE-IT phase-3 clinical trial alongside a long list of other NASH drug candidates, we propose that such capacity might be of particular relevance and potential translational benefit in contexts where intestinal MP is known to profoundly shape disease progression. Additionally, it is plausible to assume that ELA might exhibit a better efficacy profile in a cohort of NASH patients with confirmed compromised gut barrier and/or other gut-related ailments which can be ultimately determined by pursuing further investigations.

#### CRediT authorship contribution statement

YM Attia conceived the project. AS El-Khatib, YM Attia, and AN Hakeem designed the experiments. AS El-Khatib and YM Attia supervised the project. YM Attia secured funding acquisition for this project. AN Hakeem performed the experiments. MM Kamal supervised and participated in the *in vitro* and western blot experiments. OA Hammam performed the histopathological and immunohistochemical investigations. YM Attia, RA Tawfiq, and BA Abdelrahman participated in performing the experiments. MM Elmazar, YM Attia, and AN Hakeem analyzed the data. AN Hakeem wrote the original draft. YM Attia and MM Elmazar reviewed and edited the original draft. All

Authors read and approved the final manuscript.

#### Conflict of interest

The authors declare that there are no conflicts of interest.

#### Acknowledgment

This work was supported by The Young Investigator Research Grant (YIRG) awarded to Yasmeeen M. Attia by The British University in Egypt (Grant #YIRG2018-16).

#### Appendix A. Supporting information

Supplementary data associated with this article can be found in the online version at doi:10.1016/j.biopha.2022.114050.

#### References

- [1] S.L. Friedman, B.A. Neuschwander-Tetri, M. Rinella, A.J. Sanyal, Mechanisms of NAFLD development and therapeutic strategies, *Nat. Med.* 24 (2018) 1–15, <https://doi.org/10.1038/s41591-018-0104-9>.
- [2] H. Tilg, T.E. Adolph, A.R. Moschen, Multiple parallel hits hypothesis in nonalcoholic fatty liver disease: revisited after a decade, *Hepatology* 73 (2021), <https://doi.org/10.1002/hep.31518>.
- [3] J. Luther, J.J. Garber, H. Khalili, M. Dave, S.S. Bale, R. Jindal, D.L. Motola, S. Luther, S. Bohr, S.W. Jeoung, V. Deshpande, G. Singh, J.R. Turner, M. L. Yarmush, R.T. Chung, S.J. Patel, Hepatic injury in nonalcoholic steatohepatitis contributes to altered intestinal permeability, *CMGH* 1 (2015), <https://doi.org/10.1016/j.jcmgh.2015.01.001>.
- [4] F. Marra, G. Svegliati-Baroni, Lipotoxicity and the gut-liver axis in NASH pathogenesis, *J. Hepatol.* 68 (2018) 280–295, <https://doi.org/10.1016/j.jhep.2017.11.014>.
- [5] P.J. Murray, Macrophage polarization, *Annu. Rev. Physiol.* 79 (2017) 541–566, <https://doi.org/10.1146/annurev-physiol-022516-034339>.





- inflammation, *Eur. J. Immunol.* 44 (2014) 3353–3367, <https://doi.org/10.1002/eji.201343981>.
- [50] D. Rajčić, A. Baumann, A. Hernández-Arriaga, A. Brandt, A. Nier, C.J. Jin, V. Sánchez, F. Jung, A. Camarinha-Silva, I. Bergheim, Citrulline supplementation attenuates the development of non-alcoholic steatohepatitis in female mice through mechanisms involving intestinal arginase, *Redox Biol.* 41 (2021), 101879, <https://doi.org/10.1016/j.redox.2021.101879>.
- [51] K.A. Kim, W. Gu, I.A. Lee, E.H. Joh, D.H. Kim, High fat diet-induced gut microbiota exacerbates inflammation and obesity in mice via the TLR4 signaling pathway, *PLoS One* 7 (2012) 1–11, <https://doi.org/10.1371/journal.pone.0047713>.
- [52] M. Utech, A.I. Ivanov, S.N. Samarin, M. Bruewer, J.R. Turner, R.J. Msrny, C. A. Parkos, A. Nusrat, Mechanism of IFN- $\gamma$ -induced endocytosis of tight junction proteins: myosin II-dependent vacuolarization of the apical plasma membrane, *Mol. Biol. Cell.* 16 (2005) 5040–5052, <https://doi.org/10.1091/mbc.e05-03-0193>.
- [53] X. Mao, R. Sun, Q. Wang, D. Chen, B. Yu, J. He, J. Yu, J. Luo, Y. Luo, H. Yan, J. Wang, H. Wang, Q. Wang, l-Isoleucine administration alleviates DSS-induced colitis by regulating TLR4/MyD88/NF- $\kappa$ B pathway in rats, *Front. Immunol.* 12 (2022), 817583, <https://doi.org/10.3389/fimmu.2021.817583>.
- [54] A. Sapone, L. de Magistris, M. Pietzak, M.G. Clemente, A. Tripathi, F. Cucca, R. Lampis, D. Kryszak, M. Carteni, M. Generoso, D. Iafusco, F. Prisco, F. Laghi, G. Riegler, R. Carratu, D. Counts, A. Fasano, Zonulin Upregulation Is Associated With Increased Gut Permeability in Subjects With Type 1 Diabetes and Their Relatives, *Diabetes.* 55 (2006) 1443–1449. <https://doi.org/10.2337/db05-1593>.
- [55] L.B. Giron, H. Dweep, X. Yin, H. Wang, M. Damra, A.R. Goldman, N. Gorman, C.S. Palmer, H.Y. Tang, M.W. Shaikh, C.B. Forsyth, R.A. Balk, N.F. Zilberstein, Q. Liu, A. Kossenkov, A. Keshavarzian, A. Landay, M. Abdel-Mohsen, Plasma Markers of Disrupted Gut Permeability in Severe COVID-19 Patients, *Front. Immunol.* 12 (2021) 1–16. <https://doi.org/10.3389/fimmu.2021.686240>.
- [56] J. Piontek, S.M. Krug, J. Protze, G. Krause, M. Fromm, Molecular architecture and assembly of the tight junction backbone, *Biochim. Biophys. Acta - Biomembr.* 1862 (2020), 183279, <https://doi.org/10.1016/j.bbmem.2020.183279>.
- [57] F. Obermeier, G. Kojouharoff, W. Hans, J. Schölmerich, V. Gross, W. Falk, Interferon-gamma (IFN- $\gamma$ )- and tumour necrosis factor (TNF)-induced nitric oxide as toxic effector molecule in chronic dextran sulphate sodium (DSS)-induced colitis in mice, *Clin. Exp. Immunol.* 116 (1999) 238–245, <https://doi.org/10.1046/j.1365-2249.1999.00878.x>.
- [58] H.E. Hollingshead, K. Morimura, M. Adachi, M.J. Kennett, A.N. Billin, T. M. Willson, F.J. Gonzalez, J.M. Peters, PPAR $\beta$ / $\delta$  protects against experimental colitis through a ligand-independent mechanism, *Dig. Dis. Sci.* 52 (2007) 2912–2919, <https://doi.org/10.1007/s10620-006-9644-9>.
- [59] T.L. Morhardt, A. Hayashi, T. Ochi, M. Quirós, S. Kitamoto, H. Nagao-Kitamoto, P. Kuffa, K. Atarashi, K. Honda, J.Y. Kao, A. Nusrat, N. Kamada, IL-10 produced by macrophages regulates epithelial integrity in the small intestine, *Sci. Rep.* 9 (2019) 1223, <https://doi.org/10.1038/s41598-018-38125-x>.
- [60] M.J.H. Girard-Madoux, J.L. Ober-Blöbaum, L.M.M. Costes, J.M. Kel, D. J. Lindenbergh-Kortleve, I. Brouwers-Haspels, A.P. Heikema, J.N. Samsom, B. E. Clausen, IL-10 control of CD11c<sup>+</sup> myeloid cells is essential to maintain immune homeostasis in the small and large intestine, *Oncotarget* 7 (2016) 32015–32030, <https://doi.org/10.18632/oncotarget.8337>.
- [61] B. Li, R. Allli, P. Vogel, T.L. Geiger, IL-10 modulates DSS-induced colitis through a macrophage-ROS-NO axis, *Mucosal Immunol.* 7 (2014) 869–878, <https://doi.org/10.1038/mi.2013.103>.
- [62] K. Takeda, B.E. Clausen, T. Kaisho, T. Tsujimura, N. Terada, I. Förster, S. Akira, Enhanced Th1 activity and development of chronic enterocolitis in mice devoid of stat3 in macrophages and neutrophils, *Immunity* 10 (1999) 39–49, [https://doi.org/10.1016/S1074-7613\(00\)80005-9](https://doi.org/10.1016/S1074-7613(00)80005-9).
- [63] D.S. Shouval, A. Biswas, J. a Goettel, K. McCann, E. Conaway, N.S. Redhu, I. D. Mascanfroni, Z. Al Adham, S. Lavoie, M. Ibourk, D.D. Nguyen, J.N. Samsom, J. C. Escher, R. Somech, B. Weiss, R. Beier, L.S. Conklin, C.L. Ebens, F.G.M.S. Santos, A.R. Ferreira, M. Sherlock, A.K. Bhan, W. Müller, J.R. Mora, F.J. Quintana, C. Klein, A.M. Muise, B.H. Horwitz, S.B. Snapper, Interleukin-10 receptor signaling in innate immune cells regulates mucosal immune tolerance and anti-inflammatory macrophage function, *Immunity* 40 (2014) 706–719, <https://doi.org/10.1016/j.immuni.2014.03.011>.
- [64] L. Williams, L. Bradley, A. Smith, B. Foxwell, Signal transducer and activator of transcription 3 is the dominant mediator of the anti-inflammatory effects of IL-10 in human macrophages, *J. Immunol.* 172 (2004) 567–576, <https://doi.org/10.4049/jimmunol.172.1.567>.
- [65] M. Kobayashi, M.N. Kweon, H. Kuwata, R.D. Schreiber, H. Kiyono, K. Takeda, S. Akira, Toll-like receptor-dependent production of IL-12p40 causes chronic enterocolitis in myeloid cell-specific Stat3-deficient mice, *J. Clin. Invest* 111 (2003) 1297–1308, <https://doi.org/10.1172/JCI200317085>.
- [66] G.L. Seim, J. Fan, A matter of time: temporal structure and functional relevance of macrophage metabolic rewiring, *Trends Endocrinol. Metab.* 33 (2022) 345–358, <https://doi.org/10.1016/j.tem.2022.02.005>.
- [67] A. Kamalian, M. Sohrabi Asl, M. Dolatshahi, K. Afshari, S. Shamshiri, N. Momeni Roudsari, S. Momtaz, R. Rahimi, M. Abdollahi, A.H. Abdolghaffari, Interventions of natural and synthetic agents in inflammatory bowel disease, modulation of nitric oxide pathways, *World J. Gastroenterol.* 26 (2020) 3365–3400, <https://doi.org/10.3748/wjg.v26.i24.3365>.
- [68] A. Baumann, D. Rajcic, A. Brandt, V. Sánchez, F. Jung, R. Staltner, A. Nier, M. Trauner, K. Staufner, I. Bergheim, Alterations of nitric oxide homeostasis as trigger of intestinal barrier dysfunction in non-alcoholic fatty liver disease, *J. Cell. Mol. Med.* 26 (2022) 1206–1218, <https://doi.org/10.1111/jcmm.17175>.
- [69] M. Jiao, F. Ren, L. Zhou, X. Zhang, L. Zhang, T. Wen, L. Wei, X. Wang, H. Shi, L. Bai, X. Zhang, S. Zheng, J. Zhang, Y. Chen, Y. Han, C. Zhao, Z. Duan, Peroxisome proliferator-activated receptor  $\alpha$  activation attenuates the inflammatory response to protect the liver from acute failure by promoting the autophagy pathway, *Cell Death Dis.* 5 (2014) 1–11, <https://doi.org/10.1038/cddis.2014.361>.
- [70] E.-L. Paukkeri, T. Leppänen, O. Sareila, K. Vuolteenaho, H. Kankaanranta, E. Moilanen, PPAR $\alpha$  agonists inhibit nitric oxide production by enhancing iNOS degradation in LPS-treated macrophages, *Br. J. Pharmacol.* 152 (2007) 1081–1091, <https://doi.org/10.1038/sj.bjp.0707477>.
- [71] P.R. Colville-Nash, S.S. Qureshi, D. Willis, D.A. Willoughby, Inhibition of inducible nitric oxide synthase by peroxisome proliferator-activated receptor agonists: correlation with induction of heme oxygenase 1, *J. Immunol.* 161 (1998) 978–984. (<http://www.jimmunol.org/content/161/2/978>).
- [72] J.I. Odegaard, R.R. Ricardo-Gonzalez, A. Red Eagle, D. Vats, C.R. Morel, M. H. Goforth, V. Subramanian, L. Mukundan, A.W. Ferrante, A. Chawla, Alternative M2 activation of kupffer cells by PPAR $\delta$  ameliorates obesity-induced insulin resistance, *Cell Metab.* 7 (2008) 496–507, <https://doi.org/10.1016/j.cmet.2008.04.003>.
- [73] P.J. Murray, T.A. Wynn, Obstacles and opportunities for understanding macrophage polarization, *J. Leukoc. Biol.* 89 (2011) 557–563, <https://doi.org/10.1189/jlb.0710409>.
- [74] H.S. Conjeevaram, B.J. McKenna, H. Kang, E.A. Oral, J. Omo, D. White, A randomized, placebo-controlled study of PPAR-alpha agonist fenofibrate in patients with nonalcoholic steatohepatitis (NASH), *Hepatology* 50 (2009).